A Novel Kinetic Assay of Mitochondrial ATP-ADP Exchange Rate Mediated by the ANT

Christos Chinopoulos, Szilvia Vajda, László Csanády, Miklós Mándi, Katalin Mathe, and Vera Adam-Vizi*
Department of Medical Biochemistry, Semmelweis University, Neurobiochemical Group, Hungarian Academy of Sciences, Szentagothai Knowledge Center, Budapest, Hungary

ABSTRACT A novel method exploiting the differential affinity of ADP and ATP to Mg^{2+} was developed to measure mitochondrial ADP-ATP exchange rate. The rate of ATP appearing in the medium after addition of ADP to energized mitochondria, is calculated from the measured rate of change in free extramitochondrial [Mg^{2+}] reported by the membrane-impermeable $5K^{+}$ salt of the Mg^{2+}-sensitive fluorescent indicator, Magnesium Green, using standard binding equations. The assay is designed such that the adenine nucleotide translocase (ANT) is the sole mediator of changes in [Mg^{2+}] in the extramitochondrial volume, as a result of ADP-ATP exchange. We also provide data on the dependence of ATP efflux rate within the 6.8–7.8 matrix pH range as a function of membrane potential. Finally, by comparing the ATP-ADP steady-state exchange rate to the amount of the ANT in rat brain synaptic, brain nonsynaptic, heart and liver mitochondria, we provide molecular turnover numbers for the known ANT isotypes.

INTRODUCTION

The adenine nucleotide translocase (ANT) catalyzes the reversible exchange of ADP for ATP with a 1:1 stoichiometry across the inner mitochondrial membrane. It is the most abundant among mitochondrial carrier family proteins, and in the heart it accounts for as much as 10% of all inner mitochondrial membrane proteins (1,2). In humans, there are four known isoforms (3,4), all encoded by nuclear DNA (1,5). Before the recent discovery of the fourth isoform (ANT-4), it was shown that rodents lack ANT-3 (T2), (6,7), but possess ANT-1 (T1) and ANT-2 (T3), sharing a sequence homology of 97–98%, at the amino acid level (6).

Besides the canonical role of ANT as an adenine nucleotide exchanger that brings ADP into mitochondria to support respiration while simultaneously supplying cytosolic energy-consuming processes with ATP, this protein has many other roles in both physiological and pathological conditions. ADP/ATP exchange through ANT is reversible (8); therefore, in cells in which mitochondrial respiration is compromised, ATP could enter mitochondria to be hydrolyzed by the—also reversible—F_0-F_1 ATPase. This process can maintain an appreciable protonmotive force (*pmf*) in the absence of a functional respiratory chain (9). In addition to transporting nucleotides, ANT is also a major conduit of the ''proton leak'' (10), a passage of protons back into the matrix which bypasses the F_0-F_1-ATPase and causes mild uncoupling. Furthermore, ANT is thought to participate in the formation of the permeability transition pore, a multicomponent protein complex comprising a mega-channel that disrupts mitochondrial integrity (11). On the other hand, the permeability transition pore can still be activated (though with elevated thresholds) in liver mitochondria lacking all ANT isoforms harvested from transgenic animals (12).

In this study, we describe the methodology to measure mitochondrial ADP-ATP exchange rate, and correlate this rate as a function of $\Delta\Psi_m$ and ΔpH.

MATERIALS AND METHODS

Isolation of mitochondria —nonsynaptic mitochondria from rat brain

Nonsynaptic mitochondria from adult rat brain were isolated on a Percoll gradient as described previously (13) with minor modifications, as described by Chinopoulos et al. (14). Male 300–350 g Sprague-Dawley rats were used. All animal procedures were carried out according to the local animal care and use committee (Egyetemi Allatkiserleti Bizottsag) guidelines.

Synaptic mitochondria from rat brain

Synaptic mitochondria from adult rat brain were isolated as described previously (15) with major modifications: Forebrains of four rats were pooled and synaptosomes were obtained as described previously (16); briefly, cortices obtained from forebrains were chopped and homogenized using a Teflon-glass homogenizer in ice-cold isolation buffer containing 0.32 M sucrose plus 5 mM Tris with pH adjusted to 7.4 (HCl). The cortex homogenate was centrifuged at 1,900 × *g* for 10 min, the pellet was discarded, and the supernatant was centrifuged at 13,300 × *g* for 20 min. The pellet was resuspended in 0.8 M sucrose plus 5 mM Tris (pH 7.4 adjusted with HCl) and centrifuged at 10,000 × *g* for 30 min. The upper fluffy layer was removed and the supernatant (synaptosomes) was diluted slowly with ice-cold distilled water to a concentration of 0.32 M (the pellet was discarded). Subsequently, the synaptosomes were pelleted by centrifugation at 31,000 × *g* for 20 min. The obtained pellet was suspended in a medium containing 225 mM mannitol, 75 mM sucrose, 5 mM Hepes, 1 mg/ml bovine serum albumin (fatty acid-free) and 1 mM EDTA with the pH adjusted to 7.4 using Tris. Chelating residual free Mg^{2+} with EDTA renders nonmitochondrial membranes exquisitely sensitive to disintegration by nitrogen cavitation. Synaptosomes (~1.5 ml of ~20 mg/ml) were placed inside a nitrogen cell disruption bomb (model 4639, Parr Instrument, Moline, IL) precooled to 4°C, and subjected to an initial pressure of 1100 psi by delivering nitrogen to the bomb interior,

Submitted October 14, 2008, and accepted for publication December 17, 2008.

*Correspondence: veronika.adam@eok.sote.hu

Editor: Robert Nakamoto.

0006-3495/09/03/2490/15 $2.00

doi: 10.1016/j.bpj.2008.12.3915

under constant stirring. As nitrogen is dissolved within membranes, bomb pressure dropped by ~50–100 psi and further nitrogen was allowed to enter the bomb to reestablish a final value of 1100 psi, which was maintained for 10 min. After this time period, bomb pressure was decreased by opening the lower valve and ~0.8 ml of the sample was recovered and mixed with an equal volume of 30% Percoll containing 225 mM mannitol, 75 mM sucrose, 5 mM Hepes, and 1 mM EGTA (pH = 7.4 using Tris) and layered on a preformed Percoll gradient (40 and 23%). Subsequently, the procedure was identical as described above for Percoll-purified mitochondria.

Mitochondria from rat liver and heart

Mitochondria from rat heart and liver were isolated as detailed previously (17), with minor modifications, as detailed by Chinopoulos et al. (18). For all types of mitochondria, protein concentration was determined using the Biuret assay.

Assessment of inner mitochondrial membrane integrity by measuring citrate synthase activity in nonsolubilized mitochondria

Citrate synthase activity was measured as described by Srere (19). 0.1 mg of mitochondria were added to a 2 ml medium containing 100 mM Tris-HCl, 0.36 mM acetyl-CoA, 0.1 mM dithionitrobenzoic acid (pH 8.0). The reaction was started by adding 0.5 mM oxaloacetate. Changes in the absorbance at 412 nm due to 5-thio-2-nitrobenzoic acid formation were monitored in a GBC UV/VIS 920 spectrophotometer at 25°C, under constant stirring. Activity was measured in the absence and in the presence of 0.1% Triton X-100 (v/v, dissolved in 100 mM Tris-HCl, pH 8.0), and calculated as μmol/min/mg protein assuming an extinction coefficient for 5-thio-2-nitrobenzoic acid, of $\varepsilon_M = 14.15\ mM^{-1} \times cm^{-1}$. Since the inner mitochondrial membrane is impermeable to both oxaloacetate and acetyl-CoA, the fraction of broken mitochondria was estimated from the amount of measured citrate synthase activity in the absence of Triton X-100, divided by the activity measured from mitochondria solubilized by this detergent.

Oxygen consumption

Mitochondrial respiration was recorded at 37°C with a Clark-type oxygen electrode (Hansatech, UK). Mitochondria (1 mg) were added to 2 ml of an incubation medium containing (in mM): KCl 8, K-gluconate 110, NaCl 10, Hepes 10, KH_2PO4 10, EGTA 0.005, mannitol 10, $MgCl_2$ 1, *N*,*N*,*N*′,*N*′-Tetramethyl-p-phenylenediamine (TMPD) 1, K-ascorbate 5, plus 0.5 mg/ml bovine serum albumin (fatty acid-free), pH 7.25. State 3 respiration was initiated by the addition of 2 mM K-ADP (stock titrated to pH = 6.9 with KOH) to the incubation medium. State 4 respiration was initiated by the addition of 4 μM carboxyatractyloside (cATR).

Mg^{2+} fluorescence

Mitochondria (1 mg) were added to 2 ml of an incubation medium containing (in mM): KCl 8, K-gluconate 110, NaCl 10, Hepes 10, KH_2PO4 10, EGTA 0.005, mannitol 10, $MgCl_2$ 1, plus 0.5 mg/ml bovine serum albumin (fatty acid-free), pH 7.25, and 2 μM Magnesium Green 5K$^+$ salt. The following three substrate combinations were used: i), 1 mM or 0.08 mM TMPD (as indicated) plus 5 mM K-ascorbate; ii), 5 mM K-glutamate plus 5 mM K-malate; or iii), 5 mM K-succinate plus 1 μM rotenone. Magnesium Green (MgG) fluorescence was recorded in a Photon Technology International (PTI) Deltascan fluorescence spectrophotometer (Lawrenceville, NJ) at a 5 Hz acquisition rate, using 506 and 530 nm excitation and emission wavelengths, respectively. MgG exhibits an extremely high quantum yield (E_M[MgG] = 75,000 $M^{-1} \times cm^{-1}$), therefore, slits were opened to widths of no more than 1 nm. Experiments were performed at 37°C. 2 mM ADP was added, and the fluorescence (F) was recorded for 25 s, followed by addition of 4 μM cATR. At the end of each experiment, minimum fluorescence (F_{min}) was measured after addition of 4 mM EDTA, followed by the recording of maximum fluorescence (F_{max}) elicited by addition of 20 mM $MgCl_2$. Free Mg^{2+} concentration ($[Mg^{2+}]_f$) was calculated from the equation

$$\left[Mg^{2+}\right]_f = \left(K_d\left(F - F_{min}\right)/\left(F_{max} - F\right)\right) - 0.055\ mM, \quad (1)$$

assuming a K_d of 0.9 mM for the MgG-Mg^{2+} complex (20). The correction term −0.055 mM is empirical, and possibly reflects chelation of other ions by EDTA that have an affinity for MgG, and alter its fluorescence. This term was needed to obtain a reliable [Mg^{2+}] estimate, as determined from calibration experiments using solutions with known, stepwise increasing, Mg^{2+} concentrations (cf. Fig. S1 *A* in the Supporting Material). An alternative means for converting MgG fluorescence to free [Mg^{2+}] was applying the power function $f = y0 + a \times x\text{^}b$ to MgG fluorescence values obtained by stepwise additions of known amounts of Mg^{2+} to a medium containing mitochondria. Adventitious Mg^{2+} contaminating the medium before Mg^{2+} addition was considered very small and encompassed in the $y0$ constant of the power function. x is for calculated free [Mg^{2+}], a and b are constants, and f represents MgG fluorescence values.

Mitochondrial membrane potential ($\Delta\Psi_m$) determination

$\Delta\Psi_m$ was estimated using fluorescence quenching of the cationic dye safranine O, due to its accumulation inside energized mitochondria (21). Mitochondria (1 mg) were added to 2 ml of an incubation medium containing (in mM) the following: KCl 8, K-gluconate 110, NaCl 10, Hepes 10, KH_2PO4 10, EGTA 0.005, mannitol 10, $MgCl_2$ 1, plus 0.5 mg/ml bovine serum albumin (fatty acid-free), pH 7.25, and 5 μM safranine O. Substrate combinations used were as mentioned above. Experiments were performed at 37°C. Fluorescence was recorded in a PTI Deltascan fluorescence spectrophotometer at a 5 Hz acquisition rate, using 495 and 585 nm excitation and emission wavelengths, respectively. To convert Safranine O fluorescence into millivolts, a voltage-fluorescence calibration curve was constructed. To this end, Safranine O fluorescence was recorded in the presence of 2 nM valinomycin and stepwise increasing [K^+] (in the 0.2–120 mM range), which allowed calculation of $\Delta\Psi_m$ by the Nernst equation, assuming a matrix [K^+] = 120 mM (21).

Mitochondrial matrix pH (pH_i) determination

pH_i of liver mitochondria was estimated as described previously (22), with minor modifications. Briefly, mitochondria (20 mg) was suspended in a 2 ml medium containing (in mM) the following: 225 mannitol, 75 sucrose, 5 Hepes, and 0.1 EGTA (pH = 7.4, using Trizma) were incubated with 50 μM 2′,7′-bis(carboxyethyl)-5,6-carboxyfluorescein (BCECF)-AM at 30°C. After 20 min, mitochondria were centrifuged at 10,600 × *g* for 3 min (at 4°C), washed once and recentrifuged. The final pellet was suspended in 0.2 ml of the same medium devoid of EGTA and kept on ice until further manipulation. Fluorescence of hydrolyzed BCECF trapped in the matrix was measured in a Hitachi F-4500 spectrofluorimeter (Hitachi High Technologies, Berkshire, UK) in a ratiometric mode, using 450/490 nm excitation and 531 nm emission wavelengths, respectively. Buffer composition and temperature were identical to that used for both $\Delta\Psi_m$ and Mg^{2+} fluorescence determinations (see above). BCECF signal was calibrated using a range of buffers of known pH in the 6.8–7.8 range, and by equilibrating matrix pH to that of the experimental volume by 250 nM Carbonyl cyanide 4-(trifluoromethoxy)phenylhydrazone plus 10 μM nigericin.

Determination of ANT content

The ANT content of mitochondria was estimated from titration curves obtained by stepwise addition of cATR to isolated mitochondria during state three respiration, as described by Schonfeld (23).

Reagents

Standard laboratory chemicals were from Sigma (St. Louis, MO). Magnesium Green was from Invitrogen. Carboxyatractyloside was from Calbiochem (San Diego, CA). P1,P5-Di (adenosine-5′) pentaphosphate (AP_5A), safranine O and valinomycin were from Sigma. SF 6847 (Tyrphostin 9, RG-50872, Malonaben, 3,5-di-tert-butyl-4-hydroxybenzylidenemalononitrile, 2,6-di-t-butyl-4-(2′,2′-dicyanovinyl)phenol) was from Biomol (catalog No. EI-215, BIOMOL GmbH, Hamburg, Germany). All mitochondrial substrate stock solutions were dissolved in bi-distilled water and titrated to pH = 7.0 with KOH, except for TMPD which was dissolved in 10 mM Hepes and then titrated to pH = 7.0 with KOH. ATP and ADP were purchased as K^+ salts of the highest purity available and titrated to pH = 6.9 with KOH.

Statistics

Data are presented as mean ± SE; significant differences between groups of data were evaluated by one way ANOVA followed by Tukey's posthoc analysis, with $p < 0.05$ considered significant. Wherever single graphs are presented, they are representative of at least four independent experiments.

RESULTS AND DISCUSSION

Rationale for using particular buffer and substrate compositions

The ATP-ADP exchange rate was determined in intact mitochondria and the incubation medium was designed to enhance the specificity and reproducibility of our method. The main modifications, as compared to ''standard'' compositions employed elsewhere in studies with isolated mitochondria, including ours (14), were i), the replacement of a large fraction of [Cl^-] with gluconate; ii), the use of 10 mM KH_2PO_4; and iii), where indicated, the high concentration (1 mM) of TMPD. Concerning the estimation of the initial ANT activity rates and the steady-state ATP-ADP exchange rates and their differences, the reader is referred to a recent comprehensive review by Martin Klingenberg (24).

Total [Cl^-] in our buffer was ~20 mM, which was within the physiological range of intracellular [Cl^-] for all tissues used as a source of mitochondria in our study. ANT is inhibited at high [Cl^-]; 140 mM Cl^- inhibits ANT activity by ~35%, whereas with 140 mM gluconate this is only ~7% (25). The combination of [Cl^-] and [gluconate] used in our buffer is unlikely to cause substantial inhibition of ANT activity (25), while maintaining isoosmolarity. Furthermore, we found that mitochondria kept in 20 mM [Cl^-] exhibit similar respiration rates and membrane potential but significantly lower steady-state rates of ROS formation, when compared to mitochondria exposed to 140 mM [Cl^-] (data not shown).

The phosphate (P_i) concentration in our assay medium was 10 mM for the following reasons: There are two P_i carrier isoforms in mitochondria with K_m values for P_i (on the external membrane surface) of 2.2 and 0.78 mM, respectively (3). The high concentration of phosphate achieves 81.97% and 92.76% saturation of the low and high-affinity P_i carrier, respectively. At lower concentrations, extramitochondrial P_i becomes rate-limiting for oxidative phosphorylation (26), whereas at saturating [P_i] the rate of P_i transport greatly exceeds the net rate of ATP synthesis (27). At [P_i] $\leq$ 3 mM ATP formation is largely dependent on the F_0-F_1-ATPase. Finally, P*i* has been shown by mathematical modeling to play a significant role in stimulating both oxidative phosphorylation and tricarboxylic acid cycle (28), as originally proposed by Bose (29); 10 mM KH_2PO_4 did not affect free [Mg^{2+}] measured by MgG (not shown). This is partly because at pH = 7.25, KH_2PO_4 dissociates to $H_2PO_4^-$ and HPO_4^{2-} ($pK_2 = 7.21$) and neither of these ions form a precipitation with Mg^{2+} (PO_4^{3-} is the only component that forms $Mg_3(PO_4)_2$ precipitate, but this ion is essentially not present at this pH ($pK_3 = 12$)). On the other hand, Mg^{2+} also forms soluble coordination compounds with phosphate anions (preferably with HPO_4^{2-}). However, chelation of Mg^{2+} by HPO_4^{2-} in the low millimolar range is negligible, since the dissociation constant for the [Mg^{2+}-HPO_4^{2-}] complex is 210 mM (30), although a much lower value has been reported elsewhere (28).

The substrates TMPD (in most cases 1 mM) plus ascorbate were chosen for the following reasons: at concentrations >0.4 mM, TMPD supports direct transfer of electrons to cytochrome oxidase (31,32), thus, the availability of cytochrome *c* (or of any upstream component of the respiratory chain) as an electron donor is no longer rate-limiting. This is advantageous, because due to harsh isolation conditions, the outer membrane of isolated mitochondria is frequently damaged, leading to a partial loss of cytochrome *c* (33). In addition, ATP-ADP steady-state exchange rates mediated by the ANT of various types of mitochondria can be normalized to their respective cytochrome oxidase activities.

The use of TMPD plus ascorbate also eliminates a possible confounding factor, due to the binding of either ADP or ATP to the matrix-facing domain of subunit IV of cytochrome oxidase regulating its activity in a *pmf*-independent manner (34). This mechanism of respiratory control does not operate when mitochondria are fueled by TMPD plus ascorbate (35). This is important for our assay using intact mitochondria, because ATP-mediated inhibition of cytochrome oxidase would decrease *pmf*, the ultimate driving force for ANT-mediated ADP/ATP exchange.

Finally, it has been shown that the fraction of ANT molecules which form functional dimers, and hence contribute to the flux control coefficient of ANT, is maximum if TMPD plus ascorbate is used to support mitochondrial respiration, as compared to other substrate combinations (36).

The importance of including bovine serum albumin in the assay medium is twofold: first, albumin binds both fatty acids and their coenzyme A esters that can inhibit ANT activity (37,38); second, fatty acids exhibit uncoupling properties plus inhibitory effects on respiratory chain components (39) that decrease *pmf* —particularly with succinate as a substrate (40).

Finally, the use of 1 mM total [Mg^{2+}] yields 0.32–0.6 mM free [Mg^{2+}] (depending on the type and amount of adenine nucleotide present in the extramitochondrial medium; see

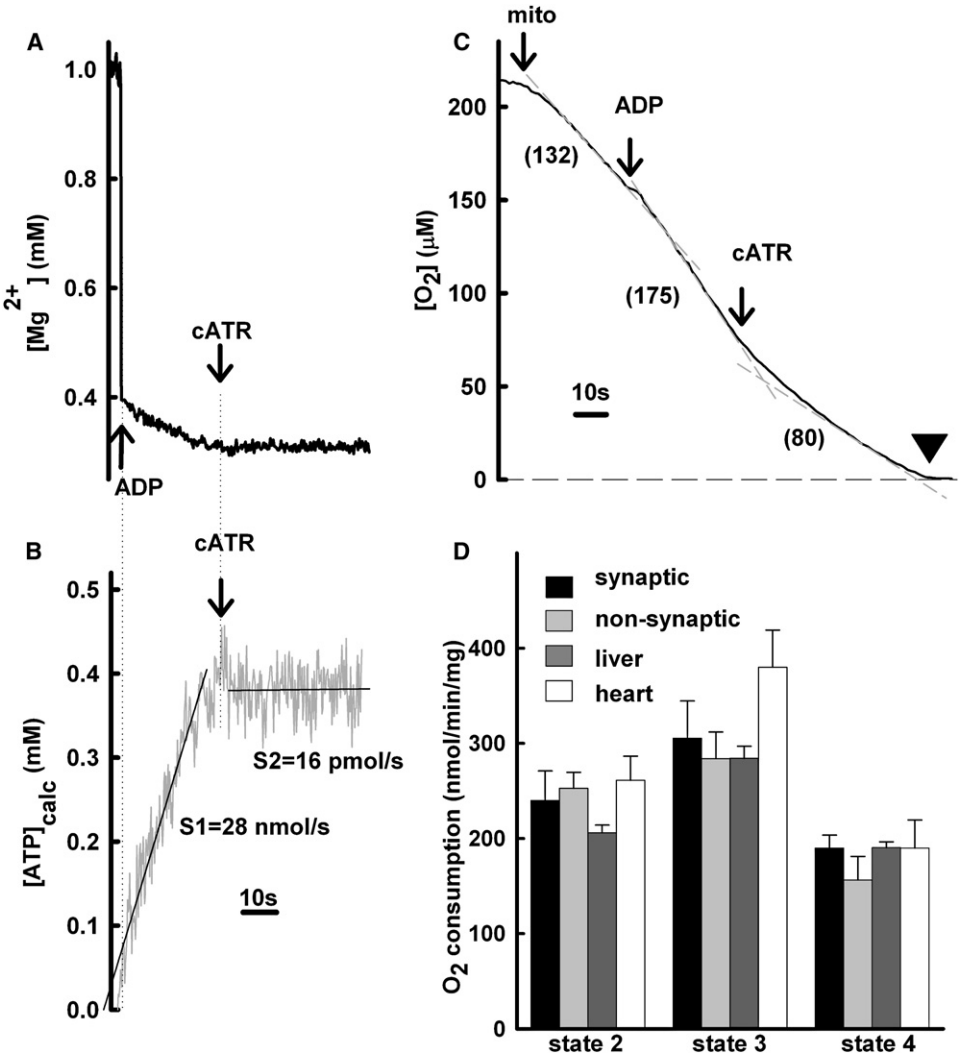

FIGURE 1 Estimation of ATP release and verification of $[O_2]$ during the experimental time frame. (*A*) Reconstructed time course of free $[Mg^{2+}]$, calculated from MgG fluorescence, using Eq. 2. Less than 50 s before the start of the trace, 1 mg of nonsynaptic mitochondria was added to a 2-ml medium containing 50 μM AP_5A, 1 mM TMPD, 5 mM ascorbate, 1 mM $MgCl_2$, and 2 μM Magnesium Green $5K^+$ salt. 2 mM ADP and 4 μM carboxy-atractyloside (cATR) were added where indicated (*arrows*). (*B*) Time course of $[ATP]_t$ appearing in the medium, calculated from the data in panel *A*, using Eq. 5. S1 and S2 are slopes obtained by linear regression ($r^2 = 0.918$ for S1, SE of the fit = 0.01). Panels *A* and *B* are aligned on the *x* axis (time, seconds). (*C*) Time course of $[O_2]$, measured with a Clark electrode in an open chamber. 1 mg of heart mitochondria, 2 mM ADP, and 4 μM cATR were sequentially added, as indicated (*arrows*), to a 2-ml medium which contained 50 μM AP_5A, 1 mM TMPD, 5 mM ascorbate, and 1 mM $MgCl_2$. Rates of respiration (μM/min) are given in parentheses. (*D*) Rates of O_2 consumption in various states of respiration, for the types of mitochondria used in this study (expressed as nmol of O_2 consumed/mg of mitochondrial protein/min). State 2 (1 mM TMPD + 5 mM ascorbate, no ADP), State 3 (substrates plus ADP), State 4 (addition of 4 μM cATR) .

below), which is within the physiological range of cytosolic free $[Mg^{2+}]$ (41–43).

Establishment of $[Mg^{2+}]$ measurement by MgG fluorescence and determination of K_d for Mg^{2+} bound to ADP or ATP under our experimental conditions

See the Supporting Material.

Estimation of ATP release in isolated mitochondria

In our assays of ATP-ADP exchange rate mediated by the ANT, we could confidently apply Eq. 5 of the Supporting Material (using $[Mg^{2+}]_t = 1$ mM, $[ADP]_t(t = 0) = 2$ mM, $[ATP]_t(t = 0) = 0$ mM, $K_{ADP} = 0.906$ mM, and $K_{ATP} = 0.114$ mM) to directly convert the recorded time course of $[Mg^{2+}]_f$ into the time course of $[ATP]_t$ in the medium (Fig. 1 *B*). The fitted slope of this time course (Fig. 1 *B*, slope *S1*) during conversion of ADP into ATP by mitochondria reflects ATP-ADP exchange rate mediated by the ANT; S2 is the slope fitted after blocking ANT operation with cATR. For all subsequent estimations of ATP-ADP exchange rate, S2 has been subtracted from S1. The standard error of the slopes given by the linear regression analysis were in the 0.01 range, and this is further assisted by the ability of the method to operate at high acquisition rate; this, in turn, enables performing the linear regression on larger number of data points and therefore, even though the data look noisy, the slope of the fit provides a robust determination of ATP production rate. For some of the experiments, the calculated initial $[ATP]_t$ values were not exactly zero, but in the range of ~0.01–0.04 mM. In these cases, we arbitrarily readjusted the calculated $[ATP]_t$ time course to make it start from zero.

Verification of the maintenance of mitochondrial respiration within the experimental time frame

Even though the experiments are performed in an open chamber, 1 mg of mitochondria in a 2 ml volume would

consume dissolved O_2 within a few minutes, especially when 1 mM TMPD plus 5 mM ascorbate is used, a combination that gives very high rates of respiration (Fig. 1 *D*). Furthermore, oxidative phosphorylation depends on oxygen tension at values lower than 100 μM [O_2] (44). To ensure that recordings of free [Mg^{2+}] are performed in mitochondria not depleted from oxygen, respiration measurements were also performed under the same conditions. As evident from Fig. 1 *C*, which shows the time course of oxygen consumption by heart mitochondria, there remained sufficient oxygen in the medium within our experimental time frame of <40 s, and, importantly, before the addition of cATR (Fig. 1 *C*), to keep cytochrome oxidase saturated. The solid arrowhead in Fig. 1 *C* indicates the time point at which [O_2] has reached the lower sensitivity limit of the Clark electrode, which is near the K_m for O_2 of cytochrome oxidase (http://www.brenda-enzymes.info/php/result_flat.php4?ecno=1.9.3.1). Among the types of mitochondria used, those isolated from heart exhibited the highest respiratory rates (Fig. 1 *D*). As cATR was given 25 s after the addition of ADP, we conclude that our experiments were not limited by oxygen depletion.

Validation of the ATP-ADP exchange rate mediated by the ANT technique

Here we describe a method to determine the ATP-ADP exchange rate mediated by the ANT in intact, metabolically competent, isolated mitochondria. The same principle should also be applicable to purified ANT protein reconstituted in liposomes (45). Because the protocol includes only a single addition of a substance (ADP), this method has the potential for a high-throughput drug screening.

The principle of the method is the measurement of the rate of the cATR-sensitive decline in free [Mg^{2+}] in the extramitochondrial compartment upon exchange of ADP with ATP. Total [ATP] in the medium is then calculated from free [Mg^{2+}] using Eq. 5 of the Supporting Material; and ATP-ADP steady-state exchange rate mediated by the ANT is expressed as total [ATP] appearing in the medium per unit time per amount of protein. This technique is viable due to the fact that ANT does not transport Mg-ADP or Mg-ATP (46,47) unlike the ATP-Mg^{2+}/Pi carrier (48), and is specific for this exchanger because all other known nucleotide transporters are insensitive to inhibition by cATR (49–53).

A conceivable limitation of our method could be the transport of Mg^{2+} across the inner mitochondrial membrane, as well as the transport of adenine nucleotides by carriers other than ANT. A mitochondrial Mg^{2+} efflux pathway of unknown molecular identity activated by cAMP has been proposed (54), but remained unconfirmed (55–57). In mammalian mitochondria, the only proven mechanisms of Mg^{2+} transport across the inner mitochondrial membrane are as follows: i), the ATP-Mg^{2+}/P_i carrier (48) and ii), a homolog of the Mrs2 protein originally described in yeast, which mediates an electrophoretic uptake of Mg^{2+} (58). Mrs2p is also found in mice, but it exhibits a low level of transcription (59). Concerning (i), free [Ca^{2+}] in our media was ~150 nM, which prevents the ATP-Mg^{2+}/Pi carrier from operation (60). Furthermore, the activity of the ATP-Mg^{2+}/Pi carrier (which can also exchange ADP unbound to Mg^{2+} for HPO_4^{2-}) (61), is manyfold lower than that of the ANT (48). To address the possible presence of Mg^{2+} transport through some Mrs2p homolog in our mitochondria, the following experiment was performed: mitochondria were incubated in a medium in the presence of substrates and cATR, but in the absence of Mg^{2+} plus 20 μM EDTA to chelate contaminating Mg^{2+}; 1 mM $MgCl_2$ was added and the rate of [Mg^{2+}] decline was recorded in the presence or absence of 0.2 μM SF 6847 (data not shown). As measured by MgG fluorescence, the rate of decline in free extramitochondrial [Mg^{2+}] was small, and not significantly affected by the presence of the uncoupler (0.00055 and 0.000462 mM/min/mg protein, respectively, in the absence and presence of the uncoupler). In contrast, the rates of decline in free, extramitochondrial [Mg^{2+}] due to ADP/ATP exchange are manyfold higher, depending on the type of mitochondria used. Based on the very low rates of decline in free, extramitochondrial [Mg^{2+}] and the lack of effect of the electrophoretic capacity of mitochondria, it is safe to assume that in our conditions, the Mrs2p—if present—contributes only insignificantly to Mg^{2+} transport. This is in agreement with the fact that in our hands, cATR abolished all changes in free [Mg^{2+}] (Fig. 1, *A* and *B*), again indicating that the ANT is the only significant means for altering extramitochondrial free [Mg^{2+}], as a result of ATP-ADP concentration changes.

When ANT molecules are reconstituted in liposomes, and there is only one of the nucleotides present in the extra- or intraliposomal, compartment, then unidirectional transport can occur (25). Otherwise, in metabolically competent, isolated mitochondria, the concerted exchange of one ADP for one ATP per ANT dimer is obligatory, ensured by the strong positive cooperativity in the binding of the two nucleotides (62,63).

The high concentration of ADP used ([ADP] falls from a 2 mM starting value to ~1.5 mM until the addition of cATR) serves two purposes. First, it ensures that ANT is saturated at all times, as its K_m for ADP is between 1 and 100 μM (3,11,64,65). In the presence of Mg^{2+}, the consensus is that the K_m for ADP is 4 μM (64). Second, State 3 respiration strongly depends on [ADP] at concentrations below 0.3 mM (66), but becomes insensitive to [ADP] above 0.5–1 mM (67). Therefore, the rate of State 3 respiration remains constant throughout the relevant part of our assay (Fig. 1 *C*).

Comparison of the present method to previously established methods for determination of ATP-ADP exchange rate mediated by the ANT

Several methods for ATP-ADP steady-state exchange rate mediated by the ANT determination have been described in

the past. Some of these directly measure ADP and/or ATP by 1), thin-layer chromatography (68); 2), high-performance liquid chromatography (69); or 3), using radioactive nucleotides (70). Others employ coupled reactions which yield an end-product that can be detected either fluorimetrically by 4), monitoring the reduction of $NADP^+$, which occurs in the presence of glucose, hexokinase, glucose-6-phosphate dehydrogenase and effluxed ATP (71,72); or 5), luminometrically, detecting chemiluminescence upon ATP-dependent oxidation of luciferin, catalyzed by firefly luciferase (73). Furthermore, there are techniques which employ fluorescent derivatives of nucleotides (method 6) to evaluate the rate of release of the fluorescent molecule upon ANT-mediated exchange for ADP (74). To complement these functional assays, the amount of ANT protein can be estimated using (method 7) a fluorescent derivative of atractyloside, or, exploiting the 1:1 stoichiometry of binding of the inhibitor to the translocase, by (method 8) stepwise titration of State 3-mitochondria with cATR until respiration is completely inhibited (23). Among these, only methods 4, 5 and perhaps 6 are on-line measurements, whereas the rest are end-point assays (although a satisfactory time resolution can be obtained using a large number of samples as detailed by Brandolin, Marty, and Vignais (75). Methods 1 and 2 require expertise in specialized equipment, whereas method 3 requires handling of radioactive material, conditions which may render these methods cumbersome to use. However, it must be noted that these are all very sensitive assays which require small amounts of mitochondrial protein. Methods 6 and 7 rely on materials which are not commercially available, and are therefore not appealing to the broader scientific community. Method 5, if used as an on-line method, suffers from several drawbacks. First, the lack of constant proportionality between ATP concentration and luminescence, caused by product inhibition of the luciferase reaction by oxyluciferin, renders this method at best semiquantitative. Second, for reliable estimation of the kinetics of ATP formation, the endogenous ATP concentration before the assay has to be determined. Third, the required use of a low ionic strength medium and room temperature restricts experiments to conditions which are nowhere near physiological. Fourth, the necessity to maintain $[O_2]$ below 50 μM, to avoid significant drifts in luminescence, adds extra effort to any application of this method. Nevertheless, some of the disadvantages of this method have been overcome by various modifications (76). Method 4 has two disadvantages. First, there are two mediating coupled reactions which may affect stoichiometry through product (glucose-6-phosphate) inhibition of hexokinase. Second, the measured signal—NADP(H) autofluorescence—precludes the simultaneous measurement of this mitochondrial parameter; plus the stimulation of mitochondrial respiration by addition of ADP affects the NAD(P)H steady state. For a comprehensive appraisal of methods to measure ATP-ADP exchange rates in mitochondria and reconstituted systems, the reader is referred to a recent review by Martin Klingenberg (24).

The advantage of the method described in our study is that it provides kinetic information at a high acquisition rate while it does not suffer from the drawbacks described for methods 4, 5 and 6. In addition, our method can be combined with simultaneous recording of further mitochondrial parameters using other types of fluorescent dyes. As an example, MgG fluorescence has been used to report changes in intracellular [ATP] in cardiomyocytes combined with simultaneous recording of NAD(P)H autofluorescence and mitochondrial membrane potential using JC-1 (20).

A disadvantage of our method is that it requires relatively large amounts of protein (1 mg per experiment was used here, although for mitochondria that exhibit high rates of ADP/ATP exchange, 0.25 mg mitochondrial protein could be sufficient). Theoretically, special cuvettes with very small internal volumes (as low as 100 μl) could be employed to decrease the amount of protein required; however, in such cases care should be taken to ensure that mitochondria do not run out of dissolved O_2 during the experiment, should the application demand full *pmf*. On the other hand, 1 mg of total mitochondrial protein contains an estimated 2–12 μg of ANT protein, depending on the source tissue (see below). Thus, in a liposome system using purified ANT, protein amounts in the low μg range should yield exchange rates in the order shown in this study, albeit lower, since transporters in reconstituted systems are prone to disorientation and partial loss of functionality.

Also, our method is not applicable for cases in which a very high concentration of Ca^{2+} (>10 μM, when at least 1 mM Mg^{2+} is present) is necessary, such as investigation of the Ca^{2+}-induced mitochondrial permeability transition (14); MgG has a K_m of 4.7 μM for Ca^{2+}, and substantial Ca^{2+} binding would alter the fluorescent signal and invalidate the calculation of free $[Mg^{2+}]$ using Eq. 1. Obviously, our method cannot be applied in the case where the integrity of the inner mitochondrial membrane has been breeched to the extent that passage of adenine nucleotides in and out of the matrix occurs freely, bypassing the obligatory exchange by the ANT.

Finally, the method described here is not applicable if one needs to exclude Mg^{2+} from the media; relevant to this, the necessity of including Mg^{2+} in the buffer could be a drawback because divalent cations (Me^{2+}), which exhibit a considerable affinity for adenine nucleotides, cause a decrease in the ATP-ADP steady-state exchange rate, exactly because of the formation of Me^{2+}-ADP and Me^{2+}-ATP complexes (47). However, the increase in the ADP-ATP steady-state exchange rate observed in the absence of Mg^{2+} compared to the rate recorded in the presence of Mg^{2+} can only be experimentally shown (24), and bears no pathophysiological relevance, as there are no conditions in situ in which cytosolic Mg^{2+} is absent. By the same token, the ADP-ATP exchange rate mediated by the ANT is strongly dependent on the $[Mg^{2+}]_f$, and it is therefore modulated by the relative concentrations of extramitochondrial $[Mg^{2+}]_t$ and its chelators, [ADP] and [ATP].

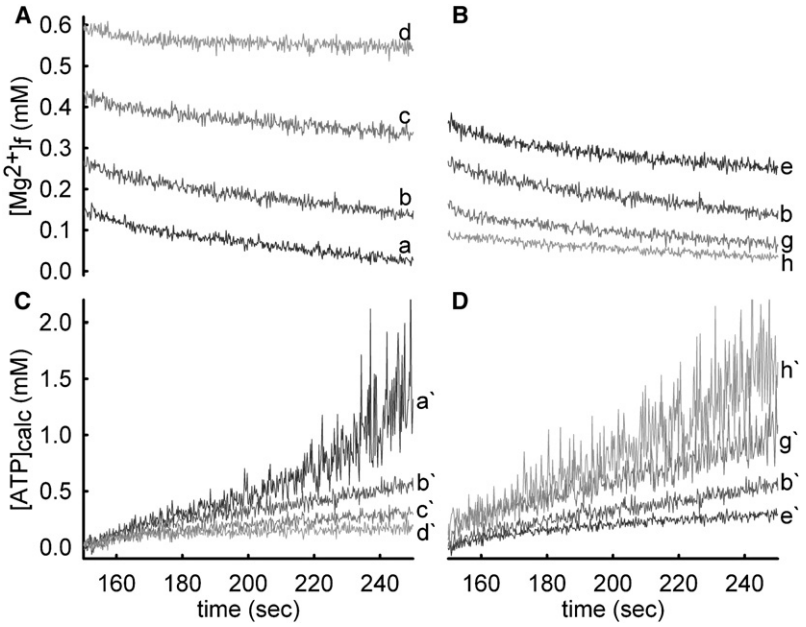

FIGURE 2 Dependence of $[Mg^{2+}]_f$ and ADP-ATP exchange rate on $[Mg^{2+}]_t$ and total [ADP]. 1 mg of liver mitochondria was added to a 2-ml medium containing 50 μM AP_5A, 5 mM K-glutamate, 5 mM K-malate, 2 μM Magnesium Green $5K^+$ salt, and $MgCl_2$ at concentrations as detailed below ($[Mg^{2+}]_t$). ADP was added at 150 s in concentrations as indicated below. (*A* and *B*) Reconstructed time course of free $[Mg^{2+}]$, calculated from MgG fluorescence, aligned on the *y* axis ($[Mg^{2+}]_f$, mM). (*C* and *D*) Time courses of corresponding $[ATP]_t$ appearing in the medium, calculated from the data in panels *A* and *B*, using Eq. 5, (aligned on the *y* axis, $[ATP]_{calc}$, mM), indicated as *a*′, *b*′, *c*′, *d*′, *e*′, *b*′, *g*′ and *h*′. All panels are aligned on the *x* axis (time, seconds). Concentrations of $[Mg^{2+}]_t$ (in mM, already present in the medium) were as follows: *a*, 0.25; *b*, 0.5; *c*, 0.75; *d*, 1. In panel *A*, 1 mM ADP was added at 150 s, whereas $[Mg^{2+}]_t$ was varied. In panel *B*, media contained 0.5 mM $MgCl_2$, and the amount of ADP added was varied as follows (in mM): *e*, 0.5; *b*, 1; *g*, 2; *h*, 4.

This is demonstrated in Fig. 2. In these experiments, rat liver mitochondria were energized with glutamate plus malate and $[Mg^{2+}]_f$ was recorded in media with increasing concentrations of $[Mg^{2+}]_t$ (0.25, 0.5, 0.75 and 1 mM; *panel A*), and adding 1 mM ADP at 150 s, or keeping $[Mg^{2+}]_t$ constant (at 0.5 mM) and altering the amount of added ADP (0.5, 1, 2, and 4 mM; *panel B*). In panel *A*, it is shown that this produced initial $[Mg^{2+}]_f$ of 0.127, 0.27, 0.429 and 0.6 mM, for *a*, *b*, *c*, and *d*, respectively. In panel *B* this produced initial $[Mg^{2+}]_f$ of 0.358, 0.27, 0.175 and 0.100 mM, for *e*, *b*, *g*, and *h*, respectively. For both *A* and *B* panels, corresponding ADP-ATP exchange rates are given in panels *C* and *D*, respectively, as *a*′, *b*′, *c*′, *d*′, *e*′, *g*′, and *h*′. As shown in panels *C* and *D*, the lower the initial $[Mg^{2+}]_f$, the higher the ADP-ATP exchange rate. However, that comes at the expense of increased noise of the calculated [ATP] appearing in the medium, due to the nature of the Eq. 5, when $[Mg^{2+}]_f$ approaches <0.1 mM values. This is a potential limitation of the method, if one wishes to investigate the ADP-ATP exchange rate at $[Mg^{2+}]_f$ below ~0.1 mM. A decrease in the signal/noise ratio will be inevitable if the initial $[Mg^{2+}]_t$ is too small, or the amount of ADP added is large enough to diminish $[Mg^{2+}]_f$ below ~0.1 mM. The effect of a gradual decreasing of $[Mg^{2+}]_f$ as a result of ADP-ATP exchange and its effect on this exchange is hard to implement, because although there is a slight initial exponential ''splay'' during the first 10 s, this is associated with an inherent decrease in $\Delta\Psi_m$ of ~25 mV (Fig. 4 *A*), and the causal relationship of ADP-ATP exchange rate to $\Delta\Psi_m$ is evident in Fig. 6 *E*. However, for the duration of the first 150 s of ADP-ATP exchange, the rate of [ATP] appearing in the medium fits well with a linear regression (Fig. 1 *B*). Therefore, the effect of the gradual change of $[Mg^{2+}]_f$ and $[ADP]_o$ cannot be discerned while the ANT is in operation. Nonetheless, the results depicted in panels 2, *C* and *D*, in which the rate of [ATP] appearing in the medium increases by increasing the initially added [ADP] or by decreasing the initially added $[Mg^{2+}]_t$, revitalize a decades-old debate: whether free Mg^{2+} affects ADP-ATP exchange rate mediated by the ANT per se, and not just through chelation of ADP only (47). Alternatively, the Km of the ANT may be higher than the currently held consensus values, which fluctuate around 0.004 mM (24). As a third—yet unexplored—possibility, ADP may be activating ANT or recruiting more ANT molecules to the mitochondrial inner membrane (see Rossignol et al. (77)).

An additional limitation of our method related to the amount of ADP and Mg^{2+} required to achieve satisfactory reproducibility, is reflected in the inability to determine the Km of the ANT for ADP or ATP. To determine the Km of the ANT, diluted suspensions of mitochondria are required (~0.07 mg/ml), concentrations of ADP in the 0.001–0.1 mM range, and concentration of Mg^{2+} in the 4 mM range. The reasons for such conditions are explained by Pfaff et al. (64), rendering our assay beyond reliable reproducibility, exactly because of the very dilute amount of functional ANTs, low ADP and high Mg^{2+}. For example, as shown in Fig. S1 *B*, addition of 0.25 mM ADP causes a 0.1097 mM decrease in $[Mg^{2+}]_f$. Since the current consensus is that the Km of ANT for ADP is ~0.004 mM, to verify that with our method, [ADP] had to be added in that range. However, that would produce a reduction in $[Mg^{2+}]_f$ smaller than the noise of the fluorescence signal. It is improbable that the method described in our manuscript can provide a reliable estimate in the low micromolar range of [ADP] values. This stems from the Km value of MgG for Mg^{2+}, which is 0.9 mM. This allows for reliable conversion of MgG fluorescence to $[Mg^{2+}]$ in the 0.1–2.5 mM range. This is depicted in Fig. S2, where a calibration curve is

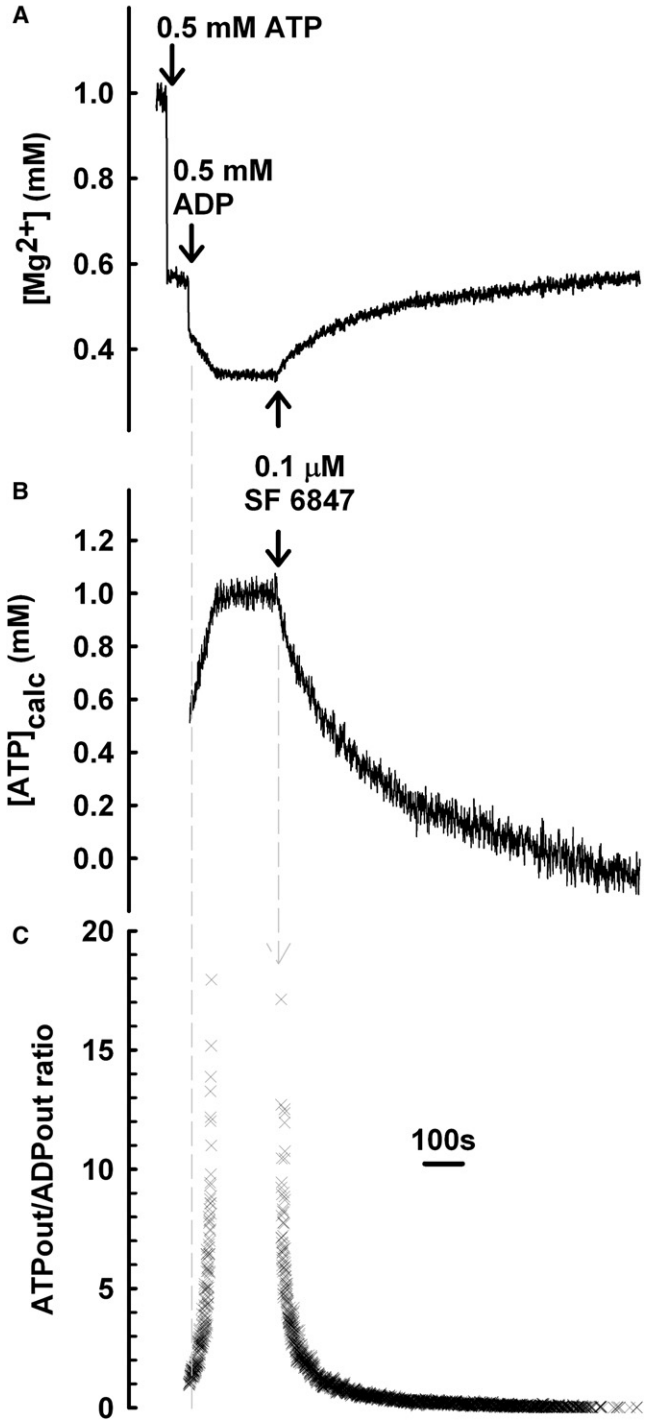

FIGURE 3 Reversibility of the ANT and estimation of extramitochondrial ATP/ADP ratio. Reconstructed time course of free $[Mg^{2+}]$, calculated from MgG fluorescence using Eq. 2. (*A*) 1 mg of liver mitochondria was added to a 2-ml medium containing 50 μM AP_5A, 5 mM K-glutamate, 5 mM K-malate, 1 mM $MgCl_2$, and 2 μM Magnesium Green $5K^+$ salt. 0.5 mM ATP and 0.5 mM ADP were added where indicated. After consumption of ADP, there is no further alteration in free $[Mg^{2+}]$. Upon addition of 0.1 μM SF 6847, a progressive elevation in free $[Mg^{2+}]$ is observed reflecting a decrease in extramitochondrial ATP and a concurrent increase in ADP. This reaction process continues until ATP is consumed. (*B*) Time course of $[ATP]_t$ in the medium, calculated from the data in panel *A* using Eq. 5. (*C*) Time course of $[ATP]_t/[ADP]_t$ in the medium, calculated from the data in panel *B* as described in the text. Panels *A*, *B*, and *C* are aligned on the *x* axis (time, seconds).

shown (sequential additions of 0.1 mM $MgCl_2$ to media containing mitochondria in the presence of ADP plus cATR). In panel A of Fig. S2, the raw trace of MgG fluorescence is shown. In panel B, a calibration curve is constructed for the entire set of data shown in panel A using a power function as described in the materials and methods. In the inset of Fig. S2 *B*, a calibration curve of the first six additions of the same calibration curve is shown that fits well with a linear regression.

Measurement of ANT in the reverse mode and estimation of the extramitochondrial ATP/ADP ratio

As mentioned above, mitochondria with a nonfunctional respiratory chain become ATP consumers, maintaining an appreciable *pmf* by pumping protons out of the matrix through the F_0-F_1-ATPase, at the expense of ATP hydrolysis. Under these conditions, the ANT reverses, bringing ATP into the matrix in exchange for ADP, driven by a $\Delta\Psi_m$ less negative than ~−100 mV. ANT reversal can also be achieved in the presence of ATP by application of an uncoupler. Consumption of ATP by mitochondria in the presence of uncouplers is a well characterized phenomenon (78). We chose to test the uncoupler SF 6847 (79), as opposed to the more widely used Carbonyl cyanide 4-(trifluoromethoxy)phenylhydrazone, Carbonyl cyanide 3-chlorophenylhydrazone, or 2, 4-dinitrophenol, because i), SF 6847 was the only uncoupler that did not quench MgG fluorescence up to a concentration of 1 μM, whereas 0.1 μM was sufficient to completely depolarize 1 mg of mitochondria. (SF 6847 is also appropriate to use with Calcium Green, a Ca^{2+}-sensitive dye, whereas all the other uncouplers tested also quenched Calcium Green fluorescence (C. Chinopoulos, unpublished observations). This is not unexpected as both Calcium Green and Magnesium Green are fluorescein derivatives); ii), the uncoupling effect of SF 6847 is resistant to cATR (80). This is important because many types of uncouplers act by inducing a proton translocation through the ANT (81), possibly jeopardizing its ability to translocate adenine nucleotides. Fig. 3 illustrates the effect of SF 6847 on ATP-ADP steady-state exchange rate mediated by the ANT. Addition of the uncoupler reversed both the time course of free $[Mg^{2+}]$ (Fig. 3 *A*), and that of $[ATP]_t$ in the extramitochondrial space (Fig. 3 *B*) demonstrating mitochondrial ATP uptake by the ANT.

As a further parameter of potential interest, our method also immediately yields the time course of the ATP/ADP ratio in the experimental volume (e.g., Fig. 3 *C*). This is because the summed concentration of ATP and ADP in the extramitochondrial compartment ($[ATP]_t + [ADP]_t$) is

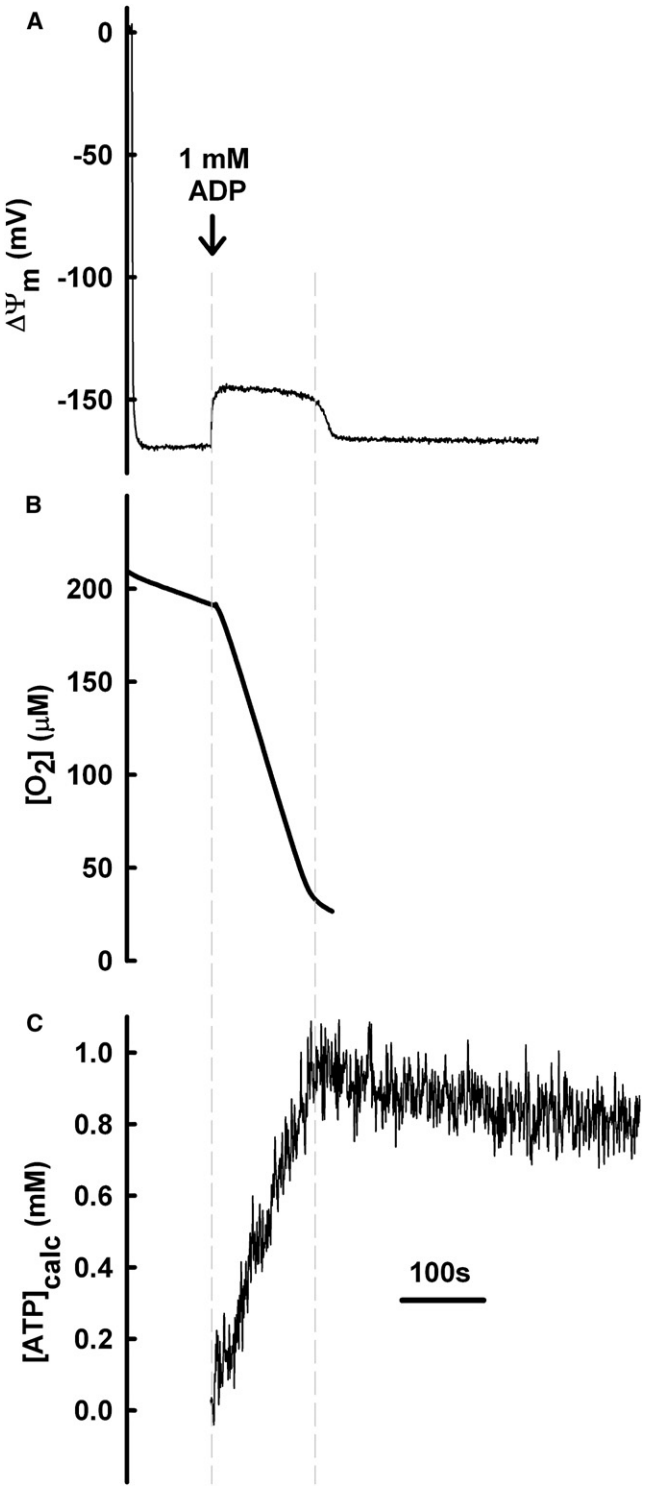

FIGURE 4 ATP-ADP exchange rate mediated by the ANT and O_2 consumption during ADP-induced depolarization. (*A*) Reconstructed time course of $\Delta\Psi_m$, calculated from safranine O fluorescence. 1 mg of liver mitochondria was added to a 2-ml medium and energized by 5 mM K-glutamate plus 5 mM K-malate. 1 mM ADP was added where indicated, causing a ~25 mV depolarization. Upon consumption of ADP, $\Delta\Psi_m$ returns to baseline level (−170 mV). (*B*) Time course of [O_2], measured with a Clark electrode in a closed chamber, using type of mitochondria and conditions as for *A*. (*C*) Time course of $[ATP]_t$ in the medium. In *B* and *C*, the same type of mitochondria and experimental conditions were used as in *A*.

known at the onset and remains constant throughout the experiment. Therefore, $[ADP]_t$ at any time point is given by $([ATP]_t(t = 0) + [ADP]_t(t = 0)) - [ATP]_t$, which affords calculation of $[ATP]_t/[ADP]_t$ (Fig. 3 *C*). Values after consumption of ADP (corresponding to plateau phase of $[ATP]_t$) are not plotted as they would reflect division by 0.

Correlation of ATP-ADP exchange rate by the ANT to ADP-induced mitochondrial membrane depolarization and state 3 respiration

Due to the electrogenic nature of the ANT (a net negative charge is exported in each ADP^{3-} import/ATP^{4-} export cycle) and because ATP formation is coupled to the flow of protons back into the matrix, initiation of state 3 respiration by addition of ADP to mitochondria is associated with a transient depolarization. This depolarization persists as long as mitochondria undergo oxidative phosphorylation. On the other hand, $\Delta\Psi_m$ contributes to the driving force for the ANT (8,46,82). Therefore, we were interested to temporally correlate ADP-induced depolarization to ATP-ADP steady-state exchange rate mediated by the ANT. As shown on Fig. 4, addition of 1 mM ADP to mitochondria causes a depolarization of 25 mV (*panel A*). The repolarization phase correlates with the transition from state 3 to state 4 respiration (indicating ADP consumption; *panel B*), as well as to cessation of changes in $[ATP]_t$ appearing in the medium (*panel C*). The fact that the oxygen consumption and $\Delta\Psi_m$ time course correlate with the calculated [ATP] time course provides additional assurance of the validity of the method.

'Normalization' of ATP-ADP exchange rate mediated by the ANT to the degree of inner mitochondrial membrane integrity

So far, the method describing the assessment of ATP-ADP exchange rate mediated by the ANT, depends on the compartmentalization of the dye, i.e., MgG must remain in the extramitochondrial medium (the $5K^+$ salt of MgG does not penetrate intact bilayers). Furthermore, the intactness of the inner mitochondrial membrane is also crucial for nucleotide translocation, as in its absence there is no *pmf* to drive i), ATP/ADP exchange; and ii), ATP formation by the F_0-F_1-ATPase. ATP-ADP exchange rate mediated by the ANT, expressed as the concentration of ATP appearing in the extramitochondrial medium per unit time per mg of mitochondrial protein, is therefore underestimated due to the presence of a fraction of damaged mitochondria (possessing a leaky inner membrane), since the latter contribute to the amount of protein but not to nucleotide translocation. We estimated the fraction of leaky mitochondria in our preparation by measuring the fractional activity of citrate synthase (a matrix enzyme) in the medium. To this end, two

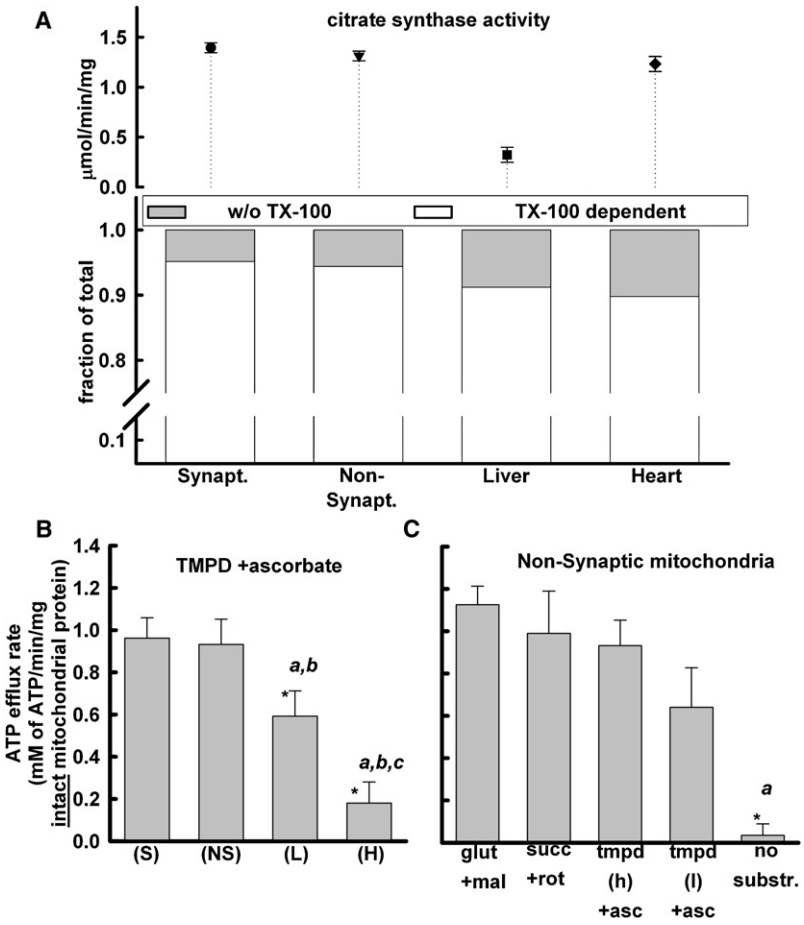

FIGURE 5 Normalization of ATP-ADP steady-state exchange rate mediated by the ANT to inner mitochondrial intactness. (*A*) Citrate synthase activity in the medium was measured for each type of mitochondrial preparation in the absence and in the presence of 0.1% Triton X-100. The top panel shows the absolute values (µmol/min/mg protein) of total citrate synthase activity, measured in the presence of 0.1% Triton X-100. In the bottom panel, shaded bars indicate the fractional activity in the absence of detergent (normalized to the total activity shown in the *top panel*); open bars plot the complementary ("TX-100 dependent") fraction. (*B*)ATP-ADP exchange rate mediated by the ANT in different types of mitochondria, normalized to the amount of intact mitochondrial protein estimated from data shown in *A*. (S), synaptic; (NS), nonsynaptic; (L), liver; (H), heart mitochondria. Mitochondria were fueled by 1 mM TMPD plus 5 mM ascorbate. (*a*, *b*) Significantly different from synaptic and nonsynaptic mitochondria ($p < 0.001$); (*c*) Significantly different from liver mitochondria ($p = 0.003$). (*C*) Normalized ATP-ADP steady-state exchange rate mediated by the ANT in nonsynaptic mitochondria fueled by a variety of mitochondrial substrates. tmpd(h) designates 1 mM TMPD; tmpd(l) designates 0.08 mM TMPD. (*a*) Significantly different from all other conditions ($p < 0.03$).

membrane-impermeable substrates, oxaloacetate and acetyl-CoA were added to the medium, and citrate synthase activity was measured as described in ''Materials and Methods''. This activity was then divided by total citrate synthase activity (Fig. 5 *A*, *top panel*), determined by repeating the measurement in the presence of 0.1% Triton X-100, which disrupts membranes. The resulting fraction is an index of the fraction of broken mitochondria (Fig. 5 *A*, *bottom panel, shaded bars*), whereas the complementary fraction indicates the fraction of intact mitochondria (Fig. 5 *A, bottom panel, open bars*) to which ATP-ADP exchange rate mediated by the ANT could be normalized. Fig. 5 *B* shows this rate normalized to the amount of intact mitochondrial protein, for each type of mitochondria fueled by 1 mM TMPD plus 5 mM ascorbate. Significantly lower activities were found in liver, and even more so in heart, as compared to brain mitochondria.

Because ATP-ADP steady-state exchange rate mediated by the ANT is driven by *pmf*, which is different depending on the substrate used for supporting respiration (83), ATP-ADP exchange rate is also expected to depend on this variable. We indeed obtained differences (Fig. 5 *C*) for nonsynaptic mitochondria fueled by different substrate combinations. However, these did not reach statistical significance, except when compared to mitochondria assayed in the complete absence of substrates.

Relationship of ATP-ADP exchange rate mediated by the ANT to cytochrome oxidase activity

When 1 mM TMPD plus 5 mM ascorbate are used as substrates for mitochondrial respiration, cytochrome oxidase is the only site at which protons are pumped out of the matrix to generate $\Delta\Psi_m$ which drives oxidative phosphorylation and ultimately ADP/ATP exchange. Consequently, cytochrome oxidase, the F_0-F_1-ATPase, and the ANT remain the only players to control the overall respiratory flux. The amount of ATPase in mitochondria of various origin could differ significantly (77). Therefore, we caution that the relative contributions of the F_0-F_1-ATPase and the ANT to the differences in ATP efflux rates among mitochondria of different origin cannot be further dissected.

By the same token, using TMPD plus ascorbate the respiratory flux of the cytochrome oxidase (and consequently of the ATPase and the ANT) likely changes (84). However, cytochrome oxidase activity can be directly measured (see Materials and Methods). This enzyme exhibits robust tissue-specific kinetic properties (85); for this and the

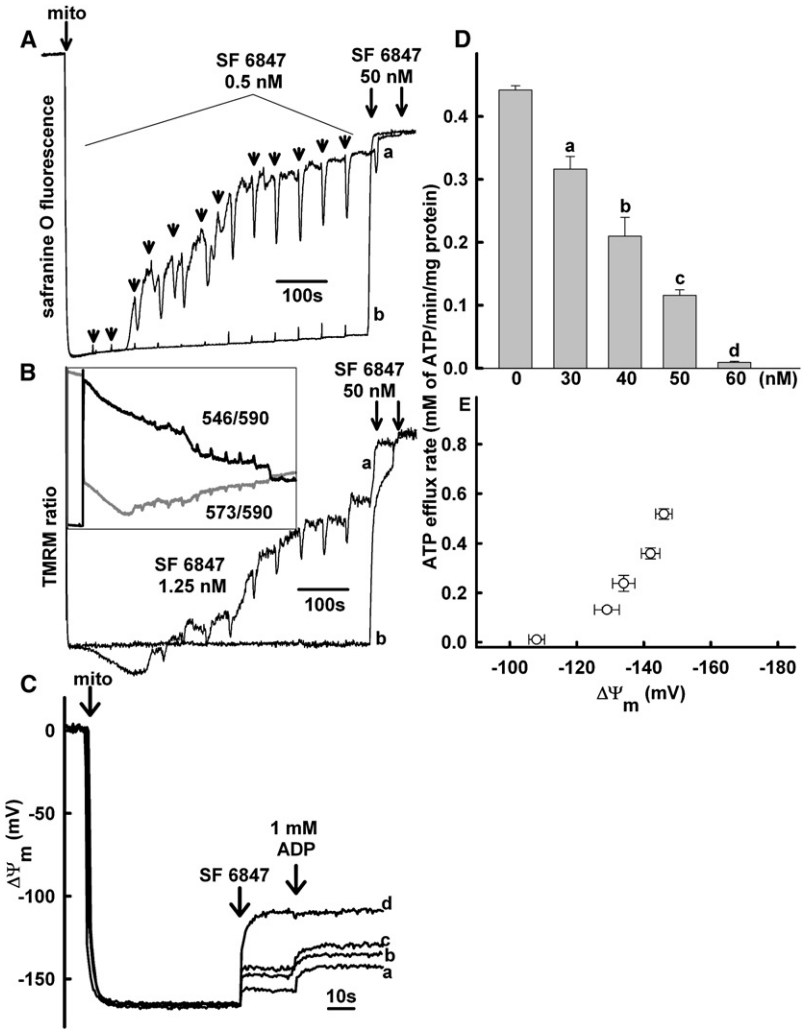

FIGURE 6 Correlation of ATP-ADP steady-state exchange rate mediated by the ANT with $\Delta\Psi_m$. (*A*) Time course of changes in safranine O fluorescence, in response to addition of SF 6847 (*small arrows*, 0.5 nM; *long arrows*, 50 nM each); 1 mg of liver mitochondria was added to a 2-ml medium and energized in curve *a*, with 1 mM TMPD plus 5 mM K-ascorbate; in curve *b*, 5 mM K-glutamate and 5 mM K-malate were added in lieu of TMPD + ascorbate. (*B*) Time course of changes in TMRM fluorescence ratio, in response to addition of SF 6847 (*small arrows*, 1.25 nM each; *long arrows*, 50 nM each); conditions identical as in *A*. (*Inset*) Time courses of individual TMRM fluorescence of 546/590 and 573/590 wavelengths used to derive the TMRM ratio shown in curve *a* of the same figure. (*C*) Time course of changes in $\Delta\Psi_m$, as calculated from safranine O fluorescence. 1 mg of liver mitochondria was added to a 2-ml medium and energized with 5 mM K-glutamate plus 5 mM K-malate. SF 6847 was added where indicated in 30 (*a*), 40 (*b*), 50 (*c*), or 60 (*d*) nM concentration. 1 mM ADP was added where indicated. (*D*) Bar graph of the ATP-ADP exchange rate mediated by the ANT measured using the same type of mitochondria and conditions as in *C*, versus the amount of uncoupler used to pretreat the mitochondria. (*E*) Plot of ATP-ADP exchange rate mediated by the ANT versus $\Delta\Psi_m$ in liver mitochondria depolarized to various voltages, constructed from the data in panels *C* and *D*. The $\Delta\Psi_m$ values represent the values obtained after addition of ADP.

previous reason, it makes sense to compare ATP-ADP exchange rates with the respective cytochrome oxidase activity (86) from various types of mitochondria. Nonetheless, no correlation between ATP-ADP exchange rates and cytochrome oxidase activity were observed (not shown).

Correlation of ATP-ADP steady-state exchange rate mediated by the ANT to $\Delta\Psi_m$

As seen on Fig. 6 *A* and *B*, mitochondria energized with TMPD plus ascorbate, were challenged by increasing concentrations of the uncoupler SF 6847. Both potentiometric dyes (Safranine O and TMRM) exhibited spikes of depolarization followed by spontaneous repolarization, sometimes unrelated to the addition of uncoupler (*curves a*). This created an obstacle for the subsequent correlation of ATP-ADP steady-state exchange rate mediated by the ANT to clamped $\Delta\Psi_m$, but it was not observed if mitochondria were energized by glutamate plus malate (*curves b*). Therefore, in subsequent experiments, mitochondria were energized with glutamate and malate, and the step size of the uncoupler concentration was increased so as to produce depolarization up to ~−100 mV (*panel C*). In parallel experiments, ATP-ADP steady-state exchange rate mediated by the ANT was measured from mitochondria pretreated with the same amount of uncoupler in the 0–60 nM range (not shown). Calculated values of ATP-ADP steady-state exchange rate mediated by the ANT were plotted versus the applied dose of the uncoupler (*panel D*). From the data shown in panels *C* and *D*, we could reconstruct the dependence of ATP-ADP steady-state exchange rate mediated by the ANT on $\Delta\Psi_m$ (*panel E*). The open circles symbols represent the $\Delta\Psi_m$ values reached 20 s after addition of ADP. In somewhat comparable conditions, rat liver mitochondria during state 3 and 4 produce similar $\Delta\Psi_m$ values (e.g., see (87)) as opposed to other kind of mitochondria, such as from pig heart (29).

Correlation of ATP-ADP steady-state exchange rate mediated by the ANT to $\Delta\Psi_m$ clamped at various matrix pH values

The ANT transports the deprotonated form of adenine nucleotides (8). We were therefore interested in how the ATP-ADP

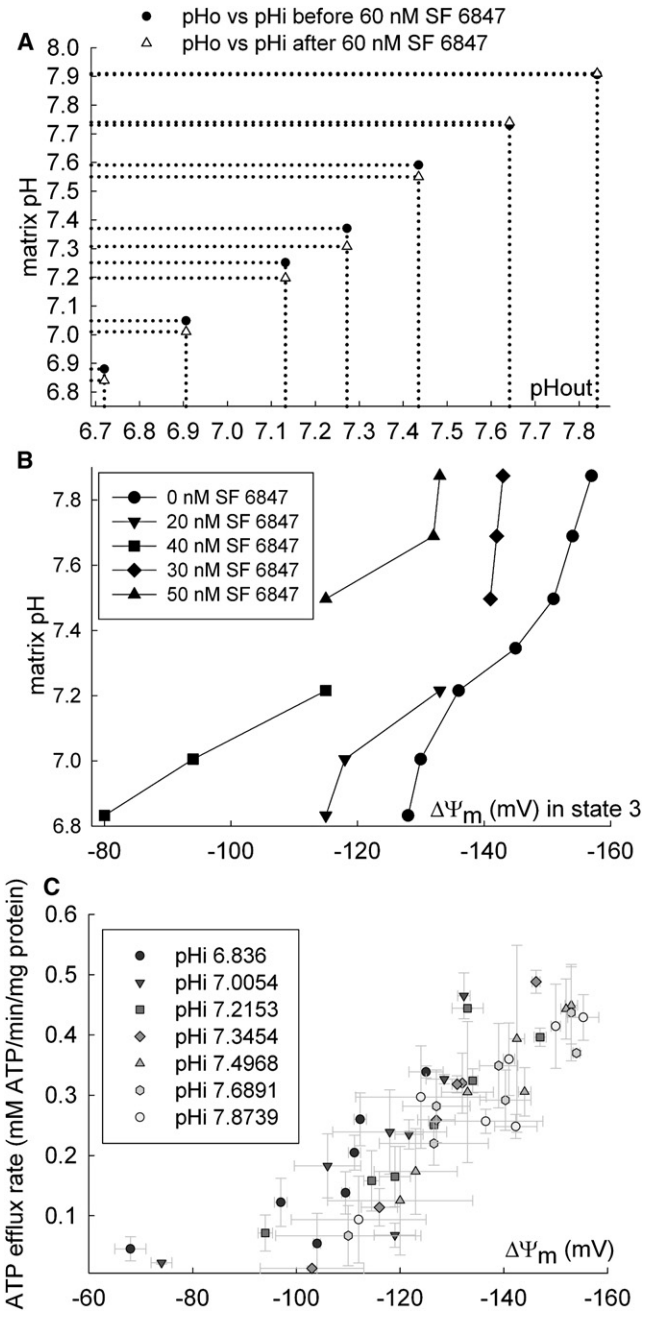

FIGURE 7 Correlation ATP-ADP steady-state exchange rate mediated by the ANT with $\Delta\Psi_m$ at various matrix pH values. (*A*) Correlation of matrix pH to the pH of the experimental volume, before and after collapse of $\Delta\Psi_m$ by SF 6847. (*B*) Correlation of matrix pH to clamped values $\Delta\Psi_m$ by titration with SF 6847 during state 3. (*C*) Correlation of ATP-ADP steady-state exchange rate mediated by the ANT with $\Delta\Psi_m$ clamped at various matrix pH values by manipulation of the pH of the experimental volume.

exchange rate depends on pH. In Fig. 7 *A*, we show a correlation diagram based on the measuring of matrix pH by calibrated BCECF ratio fluorescence to the pH of the extracellular volume. Note also that the presence of 60 nM SF 6847, a concentration that brings a complete collapse of $\Delta\Psi_m$ does not alter matrix pH significantly. Note also that at least in our experimental conditions, ΔpH_{max} is only ~0.11. In panel *B*, a correlation of measured $\Delta\Psi_m$ during state three is depicted as a function of matrix pH, in the absence (*solid circles*) or presence of uncoupler at various concentrations. Note that at higher pH values than 7.35 (pHout = 7.25), state four to state three transition causes smaller depolarization, whereas the opposite is observed for matrix pH values more acidic than 7.35. This is in good agreement with a mitochondrial energetics model described recently by the group of Beard (28). In the same panel, it is also apparent that a smaller amount of uncoupler is required at pHin < 7.35 to cause depolarization than at pHin > 7.35. This is because the efficiency of any protonophoric uncoupler (U) exhibits pH dependence. SF 6847 possesses a $pK_a = 6.5$. By increasing the pH, one increases the amount of the dissociated, U-form of uncoupler outside mitochondria, therefore more uncoupler is needed to maintain the same level of uncoupling (proton flux), since U-form does not accumulate in mitochondria. By decreasing the pH, the opposite is observed—increasing of the UH form, so less uncoupler is needed. In panel *C*, the ATP-ADP exchange rate mediated by the ANT for various matrix pH values is depicted as a function of $\Delta\Psi_m$. For panel *C*, the dissociation constants of the adenine nucleotides for Mg^{2+} for the quantification of ATP-ADP exchange rates have been reestimated for each pH value (not shown). Likewise, calibrations of safranine O for the same pH range exhibited no deviations among different pH buffer values in the −170–40 mV range (not shown).

Estimation of the molecular turnover number of the ANT

Using previously published values and our own estimates of the total amount of ANT protein found in mitochondria of various origins (0.2–0.24 nmol ANT per mg of total mitochondrial protein in liver (86,88), 1.2 nmol in heart (11), 1.44 nmol in brain nonsynaptic mitochondria (our estimate) and 1.37 nmol in synaptic mitochondria (our estimate)), we can calculate the rates of ADP/ATP exchange per ANT molecule. The calculated values of the ATP/ADP turnover rates for the ANT are between 82 s^{-1} and 99 s^{-1} in liver, are 23 s^{-1} in brain (synaptic mitochondria), 22 s^{-1} in brain (nonsynaptic), but are only 5 s^{-1} in heart. It is of note that by using substrates such as glutamate and malate, as opposed to TMPD plus ascorbate, heart mitochondria exhibit much higher ANT molecular turnover numbers (data not shown). The reasons for this phenomenon are currently being actively pursued.

These values correspond to the ''forward'' mode of transport of the ANT and are valid at 37°C, pH_o 7.25, with TMPD (1 mM) plus ascorbate (5 mM) as substrates at a $\Delta\Psi_m$ of -163 ± 3 mV (liver mitochondria), -165 ± 2 mV (heart mitochondria), -168 ± 3 mV (synaptic mitochondria), and -167 ± 3 mV (nonsynaptic mitochondria) in the presence of 1 mM total extramitochondrial Mg^{2+}.

SUPPORTING MATERIAL

Methods, equations, figures, and references are available at http://www.biophysj.org/biophysj/supplemental/S0006-3495(09)00379-8.

The authors express thanks to Drs. Anatoly A. Starkov, Ákos A. Gerencsér, Lucian Soane, Attila Ambrus, Béata Töröcsik, and Pál Bauer for helpful comments during the preparation of the manuscript; to Dr. Zsolt Vajda for help with the Scion Image software; and to András Máthé for generation of the $[Mg^{2+}]_f$-to [ATP]calc exe code.

This work was supported by the Semmelweis University Research Grant 63320, OTKA-NKTH Grant NF68294 to C.C., and by grants from OTKA, MTA, NKTH, and ETT to V.A.V.

Authors Christos Chinopoulos; Szilvia Vajda; László Csanády; and Vera Adam-Vizi (all sharing equal royalties) have filed a Patent Cooperation Treaty application regarding the ATP-ADP steady-state exchange rate mediated by the ANT assay described in this article.

REFERENCES

1. Nury, H., C. Dahout-Gonzalez, V. Trezeguet, G. J. Lauquin, G. Brandolin, et al. 2006. Relations between structure and function of the mitochondrial ADP/ATP carrier. *Annu. Rev. Biochem.* 75:713–741.
2. Pebay-Peyroula, E., and G. Brandolin. 2004. Nucleotide exchange in mitochondria: insight at a molecular level. *Curr. Opin. Struct. Biol.* 14:420–425.
3. Palmieri, F. 2004. The mitochondrial transporter family (SLC25): physiological and pathological implications. *Pflugers Arch.* 447:689–709.
4. Dolce, V., P. Scarcia, D. Iacopetta, and F. Palmieri. 2005. A fourth ADP/ATP carrier isoform in man: identification, bacterial expression, functional characterization and tissue distribution. *FEBS Lett.* 579:633–637.
5. Dahout-Gonzalez, C., H. Nury, V. Trezeguet, G. J. Lauquin, E. Pebay-Peyroula, et al. 2006. Molecular, functional, and pathological aspects of the mitochondrial ADP/ATP carrier. *Physiology (Bethesda).* 21:242–249.
6. Levy, S. E., Y. S. Chen, B. H. Graham, and D. C. Wallace. 2000. Expression and sequence analysis of the mouse adenine nucleotide translocase 1 and 2 genes. *Gene.* 254:57–66.
7. Dummler, K., S. Muller, and H. J. Seitz. 1996. Regulation of adenine nucleotide translocase and glycerol 3-phosphate dehydrogenase expression by thyroid hormones in different rat tissues. *Biochem. J.* 317:913–918.
8. Metelkin, E., I. Goryanin, and O. Demin. 2006. Mathematical modeling of mitochondrial adenine nucleotide translocase. *Biophys. J.* 90:423–432.
9. Scott, I. D., and D. G. Nicholls. 1980. Energy transduction in intact synaptosomes. Influence of plasma-membrane depolarization on the respiration and membrane potential of internal mitochondria determined in situ. *Biochem. J.* 186:21–33.
10. Brand, M. D., J. L. Pakay, A. Ocloo, J. Kokoszka, D. C. Wallace, et al. 2005. The basal proton conductance of mitochondria depends on adenine nucleotide translocase content. *Biochem. J.* 392:353–362.
11. Halestrap, A. P., and C. Brennerb. 2003. The adenine nucleotide translocase: a central component of the mitochondrial permeability transition pore and key player in cell death. *Curr. Med. Chem.* 10:1507–1525.
12. Kokoszka, J. E., K. G. Waymire, S. E. Levy, J. E. Sligh, J. Cai, et al. 2004. The ADP/ATP translocator is not essential for the mitochondrial permeability transition pore. *Nature.* 427:461–465.
13. Sims, N. R. 1990. Rapid isolation of metabolically active mitochondria from rat brain and subregions using Percoll density gradient centrifugation. *J. Neurochem.* 55:698–707.
14. Chinopoulos, C., A. A. Starkov, and G. Fiskum. 2003. Cyclosporin A-insensitive permeability transition in brain mitochondria: inhibition by 2-aminoethoxydiphenyl borate. *J. Biol. Chem.* 278:27382–27389.
15. Brown, M. R., P. G. Sullivan, K. A. Dorenbos, E. A. Modafferi, J. W. Geddes, et al. 2004. Nitrogen disruption of synaptoneurosomes: an alternative method to isolate brain mitochondria. *J. Neurosci. Methods.* 137:299–303.
16. Adam-Vizi, V., and E. Ligeti. 1984. Release of acetylcholine from rat brain synaptosomes by various agents in the absence of external calcium ions. *J. Physiol.* 353:505–521.
17. Tyler, D. D., and J. Gonze. 1967. The preparation of heart mitochondria from laboratory animals. *Methods Enzymol.* 10:75–77.
18. Chinopoulos, C., A. A. Starkov, S. Grigoriev, L. M. Dejean, K. W. Kinnally, et al. 2005. Diacylglycerols Activate Mitochondrial Cationic Channel(s) and Release Sequestered Ca(2+). *J. Bioenerg. Biomembr.* 37:237–247.
19. Srere, P. A. 1969, Citrate synthase and J. M. Lowenstein, editors. Academic Press, New York. 3–11.
20. Leyssens, A., A. V. Nowicky, L. Patterson, M. Crompton, and M. R. Duchen. 1996. The relationship between mitochondrial state, ATP hydrolysis, [Mg2+]i and [Ca2+]i studied in isolated rat cardiomyocytes. *J. Physiol.* 496:111–128.
21. Akerman, K. E., and M. K. Wikstrom. 1976. Safranine as a probe of the mitochondrial membrane potential. *FEBS Lett.* 68:191–197.
22. Zolkiewska, A., A. Czyz, J. Duszynski, and L. Wojtczak. 1993. Continuous recording of intramitochondrial pH with fluorescent pH indicators: novel probes and limitations of the method. *Acta Biochim. Pol.* 40: 241–250.
23. Schonfeld, P. 1990. Does the function of adenine nucleotide translocase in fatty acid uncoupling depend on the type of mitochondria? *FEBS Lett.* 264:246–248.
24. Klingenberg, M. 2008. The ADP and ATP transport in mitochondria and its carrier. *Biochim. Biophys. Acta.* 1778:1978–2021.
25. Gropp, T., N. Brustovetsky, M. Klingenberg, V. Muller, K. Fendler, et al. 1999. Kinetics of electrogenic transport by the ADP/ATP carrier. *Biophys. J.* 77:714–726.
26. Tager, J. M., R. J. Wanders, A. K. Groen, W. Kunz, R. Bohnensack, et al. 1983. Control of mitochondrial respiration. *FEBS Lett.* 151:1–9.
27. Ligeti, E., G. Brandolin, Y. Dupont, and P. V. Vignais. 1985. Kinetics of Pi-Pi exchange in rat liver mitochondria. Rapid filtration experiments in the millisecond time range. *Biochemistry.* 24:4423–4428.
28. Wu, F., F. Yang, K. C. Vinnakota, and D. A. Beard. 2007. Computer modeling of mitochondrial tricarboxylic acid cycle, oxidative phosphorylation, metabolite transport, and electrophysiology. *J. Biol. Chem.* 282:24525–24537.
29. Bose, S., S. French, F. J. Evans, F. Joubert, and R. S. Balaban. 2003. Metabolic network control of oxidative phosphorylation: multiple roles of inorganic phosphate. *J. Biol. Chem.* 278:39155–39165.
30. Dawson, R. M. C., D. C. Elliot, W. H. Elliot, and K. M. Jones. 1986. Data for Biochemical Research. Clarendon Press, Oxford.
31. Sagi-Eisenberg, R., and M. Gutman. 1979. Generation of high delta psi in respiring submitochondrial particles by steady-state accumulation of oxidized *N*,*N*,*N*′,*N*′-tetramethyl-p-phenylenediamine. *Eur. J. Biochem.* 97:127–132.
32. Crinson, M., and P. Nicholls. 1992. Routes of electron transfer in beef heart cytochrome *c* oxidase: is there a unique pathway used by all reductants? *Biochem. Cell Biol.* 70:301–308.
33. Wojtczak, L., H. Zaluska, A. Wroniszewska, and A. B. Wojtczak. 1972. Assay for the intactness of the outer membrane in isolated mitochondria. *Acta Biochim. Pol.* 19:227–234.
34. Kadenbach, B., and S. Arnold. 1999. A second mechanism of respiratory control. *FEBS Lett.* 447:131–134.
35. Arnold, S., and B. Kadenbach. 1997. Cell respiration is controlled by ATP, an allosteric inhibitor of cytochrome-*c* oxidase. *Eur. J. Biochem.* 249:350–354.
36. Faustin, B., R. Rossignol, C. Rocher, G. Benard, M. Malgat, et al. 2004. Mobilization of adenine nucleotide translocators as molecular bases of the biochemical threshold effect observed in mitochondrial diseases. *J. Biol. Chem.* 279:20411–20421.

37. Wojtczak, L., and H. Zaluska. 1967. The inhibition of translocation of adenine nucleotides through mitochondrial membranes by oleate. *Biochem. Biophys. Res. Commun.* 28:76–81.
38. Morel, F., G. Lauquin, J. Lunardi, J. Duszynski, and P. V. Vignais. 1974. An appraisal of the functional significance of the inhibitory effect of long chain acyl-CoAs on mitochondrial transports. *FEBS Lett.* 39:133–138.
39. Wojtczak, L., and P. Schonfeld. 1993. Effect of fatty acids on energy coupling processes in mitochondria. *Biochim. Biophys. Acta.* 1183:41–57.
40. Tretter, L., D. Mayer-Takacs, and V. Adam-Vizi. 2007. The effect of bovine serum albumin on the membrane potential and reactive oxygen species generation in succinate-supported isolated brain mitochondria. *Neurochem. Int.* 50:139–147.
41. Rodriguez-Zavala, J. S., and R. Moreno-Sanchez. 1998. Modulation of oxidative phosphorylation by Mg2+ in rat heart mitochondria. *J. Biol. Chem.* 273:7850–7855.
42. Rutter, G. A., N. J. Osbaldeston, J. G. McCormack, and R. M. Denton. 1990. Measurement of matrix free Mg2+ concentration in rat heart mitochondria by using entrapped fluorescent probes. *Biochem. J.* 271:627–634.
43. Jung, D. W., E. Panzeter, K. Baysal, and G. P. Brierley. 1997. On the relationship between matrix free Mg2+ concentration and total $Mg2^{+}$ in heart mitochondria. *Biochim. Biophys. Acta.* 1320:310–320.
44. Wilson, D. F., C. S. Owen, and M. Erecinska. 1979. Quantitative dependence of mitochondrial oxidative phosphorylation on oxygen concentration: a mathematical model. *Arch. Biochem. Biophys.* 195:494–504.
45. Kramer, R. 1986. Reconstitution of ADP/ATP translocase in phospholipid vesicles. *Methods Enzymol.* 125:610–618.
46. Klingenberg, M. 1980. The ADP-ATP translocation in mitochondria, a membrane potential controlled transport. *J. Membr. Biol.* 56:97–105.
47. Kramer, R. 1980. Influence of divalent cations on the reconstituted ADP, ATP exchange. *Biochim. Biophys. Acta.* 592:615–620.
48. Aprille, J. R. 1993. Mechanism and regulation of the mitochondrial ATP-Mg/P(i) carrier. *J. Bioenerg. Biomembr.* 25:473–481.
49. Vozza, A., E. Blanco, L. Palmieri, and F. Palmieri. 2004. Identification of the mitochondrial GTP/GDP transporter in *Saccharomyces cerevisiae*. *J. Biol. Chem.* 279:20850–20857.
50. Dolce, V., G. Fiermonte, M. J. Runswick, F. Palmieri, and J. E. Walker. 2001. The human mitochondrial deoxynucleotide carrier and its role in the toxicity of nucleoside antivirals. *Proc. Natl. Acad. Sci.* 98:2284–2288.
51. Fiermonte, G., L. F. De, S. Todisco, L. Palmieri, F. M. Lasorsa, et al. 2004. Identification of the mitochondrial ATP-Mg/Pi transporter. Bacterial expression, reconstitution, functional characterization, and tissue distribution. *J. Biol. Chem.* 279:30722–30730.
52. Palmieri, L., H. Rottensteiner, W. Girzalsky, P. Scarcia, F. Palmieri, et al. 2001. Identification and functional reconstitution of the yeast peroxisomal adenine nucleotide transporter. *EMBO J.* 20:5049–5059.
53. Shin, S. J., W. K. Lee, H. W. Lim, and J. Park. 2000. Characterization of the ATP transporter in the reconstituted rough endoplasmic reticulum proteoliposomes. *Biochim. Biophys. Acta.* 1468:55–62.
54. Romani, A., E. Dowell, and A. Scarpa. 1991. Cyclic AMP-induced Mg2+ release from rat liver hepatocytes, permeabilized hepatocytes, and isolated mitochondria. *J. Biol. Chem.* 266:24376–24384.
55. Altschuld, R. A., D. W. Jung, R. M. Phillips, P. Narayan, L. C. Castillo, et al. 1994. Evidence against norepinephrine-stimulated efflux of mitochondrial Mg2+ from intact cardiac myocytes. *Am. J. Physiol.* 266:H1103–H1111.
56. Bernardi, P. 1999. Mitochondrial transport of cations: channels, exchangers, and permeability transition. *Physiol. Rev.* 79:1127–1155.
57. Murphy, E. 2000. Mysteries of magnesium homeostasis. *Circ. Res.* 86:245–248.
58. Kolisek, M., G. Zsurka, J. Samaj, J. Weghuber, R. J. Schweyen, et al. 2003. Mrs2p is an essential component of the major electrophoretic Mg2+ influx system in mitochondria. *EMBO J.* 22:1235–1244.
59. Zsurka, G., J. Gregan, and R. J. Schweyen. 2001. The human mitochondrial Mrs2 protein functionally substitutes for its yeast homologue, a candidate magnesium transporter. *Genomics.* 72:158–168.
60. Nosek, M. T., D. T. Dransfield, and J. R. Aprille. 1990. Calcium stimulates ATP-Mg/Pi carrier activity in rat liver mitochondria. *J. Biol. Chem.* 265:8444–8450.
61. Nosek, M. T., and J. R. Aprille. 1992. ATP-Mg/Pi carrier activity in rat liver mitochondria. *Arch. Biochem. Biophys.* 296:691–697.
62. Duyckaerts, C., C. M. Sluse-Goffart, J. P. Fux, F. E. Sluse, and C. Liebecq. 1980. Kinetic mechanism of the exchanges catalysed by the adenine-nucleotide carrier. *Eur. J. Biochem.* 106:1–6.
63. Barbour, R. L., and S. H. Chan. 1981. Characterization of the kinetics and mechanism of the mitochondrial ADP-atp carrier. *J. Biol. Chem.* 256:1940–1948.
64. Pfaff, E., H. W. Heldt, and M. Klingenberg. 1969. Adenine nucleotide translocation of mitochondria. Kinetics of the adenine nucleotide exchange. *Eur. J. Biochem.* 10:484–493.
65. Akerboom, T. P., H. Bookelman, and J. M. Tager. 1977. Control of ATP transport across the mitochondrial membrane in isolated rat-liver cells. *FEBS Lett.* 74:50–54.
66. Jacobus, W. E., R. W. Moreadith, and K. M. Vandegaer. 1982. Mitochondrial respiratory control. Evidence against the regulation of respiration by extramitochondrial phosphorylation potentials or by [ATP]/[ADP] ratios. *J. Biol. Chem.* 257:2397–2402.
67. Kay, L., K. Nicolay, B. Wieringa, V. Saks, and T. Wallimann. 2000. Direct evidence for the control of mitochondrial respiration by mitochondrial creatine kinase in oxidative muscle cells in situ. *J. Biol. Chem.* 275:6937–6944.
68. Pedersen, P. L., and W. A. Catterall. 1979. The use of thin-layer chromatography on poly(ethyleneimine) cellulose to facilitate assays of ATP-ADP exchange, ATP-Pi exchange, adenylate kinase, and nucleoside diphosphokinase activity. *Methods Enzymol.* 55:283–289.
69. Hartwick, R. A., and P. R. Brown. 1975. The performance of microparticle chemically-bonded anion-exchange resins in the analysis of nucleotides. *J. Chromatogr.* 112:650–662.
70. Duee, E. D., and P. V. Vignais. 1969. Kinetics and specificity of the adenine nucleotide translocation in rat liver mitochondria. *J. Biol. Chem.* 244:3920–3931.
71. Williamson, J. R., and B. E. Corkey. 1979. Assay of citric acid cycle intermediates and related compounds–update with tissue metabolite levels and intracellular distribution. *Methods Enzymol.* 55:200–222.
72. Passarella, S., A. Ostuni, A. Atlante, and E. Quagliariello. 1988. Increase in the ADP/ATP exchange in rat liver mitochondria irradiated in vitro by helium-neon laser. *Biochem. Biophys. Res. Commun.* 156:978–986.
73. Lemasters, J. J., and C. R. Hackenbrock. 1979. Continuous measurement of adenosine triphosphate with firefly luciferase luminescence. *Methods Enzymol.* 56:530–544.
74. Block, M. R., F. Boulay, G. Brandolin, Y. Dupont, G. J. Lauquin, et al. 1986. Fluorescent probes of the mitochondrial ADP/ATP carrier protein. *Methods Enzymol.* 125:639–649.
75. Brandolin, G., I. Marty, and P. V. Vignais. 1990. Kinetics of nucleotide transport in rat heart mitochondria studied by a rapid filtration technique. *Biochemistry.* 29:9720–9727.
76. Wibom, R., A. Lundin, and E. Hultman. 1990. A sensitive method for measuring ATP-formation in rat muscle mitochondria. *Scand. J. Clin. Lab. Invest.* 50:143–152.
77. Rossignol, R., T. Letellier, M. Malgat, C. Rocher, and J. P. Mazat. 2000. Tissue variation in the control of oxidative phosphorylation: implication for mitochondrial diseases. *Biochem. J.* 347:45–53.
78. Budd, S. L., and D. G. Nicholls. 1996. A reevaluation of the role of mitochondria in neuronal $Ca2^{+}$ homeostasis. *J. Neurochem.* 66:403–411.
79. Terada, H. 1981. The interaction of highly active uncouplers with mitochondria. *Biochim. Biophys. Acta.* 639:225–242.
80. Skulachev, V. P. 1998. Uncoupling: new approaches to an old problem of bioenergetics. *Biochim. Biophys. Acta.* 1363:100–124.

81. Lou, P. H., B. S. Hansen, P. H. Olsen, S. Tullin, M. P. Murphy, et al. 2007. Mitochondrial uncouplers with an extraordinary dynamic range. *Biochem. J.* 407:129–140.

82. Alexandre, A., B. Reynafarje, and A. L. Lehninger. 1978. Stoichiometry of vectorial H^+ movements coupled to electron transport and to ATP synthesis in mitochondria. *Proc. Natl. Acad. Sci. USA.* 75:5296–5300.

83. Lee, C. P., Q. Gu, Y. Xiong, R. A. Mitchell, and L. Ernster. 1996. P/O ratios reassessed: mitochondrial P/O ratios consistently exceed 1.5 with succinate and 2.5 with NAD-linked substrates. *FASEB J.* 10:345–350.

84. Brand, M. D., B. P. Vallis, and A. Kesseler. 1994. The sum of flux control coefficients in the electron-transport chain of mitochondria. *Eur. J. Biochem.* 226:819–829.

85. Patel, S. P., and S. S. Katyare. 2005. Differences in kinetic properties of cytochrome oxidase in mitochondria from rat tissues. A comparative study. *Z. Naturforsch.* [*C.*] 60:785–791.

86. Forman, N. G., and D. F. Wilson. 1983. Dependence of mitochondrial oxidative phosphorylation on activity of the adenine nucleotide translocase. *J. Biol. Chem.* 258:8649–8655.

87. Azzu, V., N. Parker, and M. D. Brand. 2008. High membrane potential promotes alkenal-induced mitochondrial uncoupling and influences adenine nucleotide translocase conformation. *Biochem. J.* 413:323–332.

88. Winkler, H. H., and A. L. Lehninger. 1968. The atractyloside-sensitive nucleotide binding site in a membrane preparation from rat liver mitochondria. *J. Biol. Chem.* 243:3000–3008.